

# The Origin of Visible Light Absorption in Chalcogen Element (S, Se, and Te)-Doped Anatase TiO<sub>2</sub> Photocatalysts

Jian Wei Zheng,<sup>\*,†</sup> Atreyee Bhattacharayya,<sup>§</sup> Ping Wu,<sup>\*,†</sup> Zhong Chen,<sup>‡</sup> James Highfield,<sup>||</sup> Zhili Dong,<sup>‡</sup> and Rong Xu<sup>§</sup>

*Institute of High Performance Computing, 1 Fusionopolis Way, #16-16 Connexis, Singapore 138632, School of Materials Science and Engineering, Nanyang Technological University, Block N4.1, Nanyang Avenue, Singapore 639798, School of Chemical & Biomedical Engineering, Nanyang Technological University, 62, Nanyang Drive, Singapore 637459, and Institute of Chemical and Engineering Sciences, 1 Pesek Road, Jurong Island, Singapore 627833*

Received: December 4, 2009; Revised Manuscript Received: March 18, 2010

We use first-principles calculations to clarify the origin of the visible light absorption in chalcogen element-doped TiO<sub>2</sub>. Our results show that interstitial doping is not the origin of visible light absorption under any equilibrium growth conditions, but rather, sensitization is achievable via substitutional doping of O (or Ti) at Ti-rich (or O-rich) conditions, respectively. With increasing atomic number (from S to Te), it is harder to form anion-doped TiO<sub>2</sub> but easier to achieve cationic doping. Both anionic and cationic doping can confer visible light absorption, but the former is more effective. The effect increases with increasing atomic number of the chalcogen element. Dopant pairing is found in anionic S-, Se-, and Te- and cationic S-doped TiO<sub>2</sub>. We further identified that anion pairing induces a bathochromic shift in the absorption, whereas cationic pairing causes the opposite, that is, a hypsochromic (blue) shift, predictions that agree well with the experimental findings.

## Introduction

There is great interest in developing photocatalysts that are not only able to split water to obtain hydrogen as a clean and renewable energy source<sup>1–4</sup> but are also effective in degrading pollutants to keep the environment clean.<sup>5</sup> However, most of photocatalysts are wide band-gap materials that are only active in the UV region. Therefore, much of the current research is devoted to the development of visible-light-active photocatalysts. Visible light accounts for about 43% of the incoming solar power as compared with just 3% for the UV. To absorb visible light, the band gap must be reduced below 3.0 eV. This has traditionally been attempted by doping metals (cations),<sup>6–11</sup> but recent interest has been shown in doping nonmetals (anions)<sup>12–27</sup> into these wide band-gap semiconductors.

Nonmetal doping (N,<sup>12–17</sup> C,<sup>18</sup> B,<sup>19</sup> halogens,<sup>20,21</sup> and S<sup>12,22–27</sup>) has been found to more consistently and effectively shift the absorption of TiO<sub>2</sub> toward the visible light region. Theoretical calculations show that an impurity state (2p for C and N, 3p for S) just above the valence band maximum (VBM), generated by substitutional anion doping, is responsible for this red (bathochromic) shift. However, there are a wide variety of possible dopant configurations in the host crystal lattice. For example, depending on the nitrification conditions, interstitial dopant atoms, substitutional dopant atoms, or complex species

(NO, NO<sub>2</sub>, N<sub>2</sub>, and NH<sub>x</sub>) can exist in N-doped TiO<sub>2</sub>.<sup>13</sup> All of these species generate gap states that could contribute to the red shift.

The origin of visible-light-active S-doped TiO<sub>2</sub> is usually thought to be linked to substitution of S for either an O or a Ti atom. Umabayashi et al<sup>22</sup> successfully synthesized S-doped TiO<sub>2</sub> by oxidizing TiS<sub>2</sub> in air and confirmed that the red shift was due to substitutional anionic S doping by X-ray photoelectron spectroscopy (XPS), X-ray diffraction (XRD), diffuse reflectance spectroscopy (DRS), and density functional theory (DFT) calculation. A high-energy peak in the XPS spectrum was ascribed to surface contamination by sulfur dioxide (SO<sub>2</sub>). Ohno et al<sup>23</sup> later adopted a sol–gel approach to synthesize S-doped TiO<sub>2</sub> by reacting titanium isopropoxide with thiourea and then calcining the gel at various temperatures. Like Umabayashi's findings, a peak assignable to S<sup>4+</sup> was found in the XPS spectrum of the product even after washing with distilled water for 1 h. Although they did not exclude the possibility that it was of interstitial type, they favored substitutional cationic S doping. In view of the small ionic radii of cationic sulfur (0.37 and 0.29 Å for S<sup>4+</sup> and S<sup>6+</sup>, respectively) and the relatively open network of anatase TiO<sub>2</sub>, interstitial S could conceivably exist. Therefore, it is interesting to model interstitial S dopants in TiO<sub>2</sub> and how they may affect the electronic structure. Moreover, sulfur atoms tend to associate with other sulfur atoms in what is termed "catenation". This is found in many ring systems of sulfur, sulfanes, and metal polysulfides. It is not yet clear whether sulfur dopants tend to pair or cluster in S-doped TiO<sub>2</sub>. To date, no experimental or theoretical work on interstitial doping and dopant pairing in S-doped TiO<sub>2</sub>, has been reported. It is also of interest to explore doping across the chalcogen element series, which is similarly unreported. It is expected that doping Se or Te into TiO<sub>2</sub> would achieve the same effect as S doping because TiSe<sub>2</sub> and TiTe<sub>2</sub> are semimetals.

\* To whom correspondence should be addressed. E-mail: zhengjw@ihpc.a-star.edu.sg (J.W.Z.), wupin@ihpc.a-star.edu.sg (P.W.). Phone: +65 6419 1567, +65-64191212. Fax: +65 64632536.

<sup>†</sup> Institute of High Performance Computing.

<sup>‡</sup> School of Materials Science and Engineering, Nanyang Technological University.

<sup>§</sup> School of Chemical & Biomedical Engineering, Nanyang Technological University.

<sup>||</sup> Institute of Chemical and Engineering Sciences.

In this paper, we use first-principles calculations to clarify the origin of visible light absorption in chalcogen element-doped anatase TiO<sub>2</sub>. We consider anionic, cationic, and interstitial doping and calculate the corresponding formation energies. According to our modeling, interstitial doping cannot remain stable under any equilibrium growth condition and can be ruled out as the origin of visible light absorption. Chalcogen elements will substitute for O atoms under Ti-rich conditions and vice versa. In this study, substitutional doping is identified as the probable cause of coloration in anatase TiO<sub>2</sub>. Finally, we consider chalcogen dopant pairing; a process that may have a profound influence upon coloration.

### Computational Details

Density functional theory (DFT) calculations were performed using the Vienna ab initio Simulation Package (VASP) program code,<sup>28,29</sup> in which a plane-wave basis set is used. The electron–ion interaction is modeled by the projector-augmented wave (PAW) method.<sup>30,31</sup> The Perdew–Wang form of generalized gradient approximation (GGA) was used for the exchange and correlation functional.<sup>32</sup> The plane-wave cutoff energy was set to 520 eV. The Monkhost–Pack *k*-point samplings were 4 × 4 × 4 for a 2 × 2 × 2 supercell and 9 × 9 × 9 for a unit cell of anatase TiO<sub>2</sub>. The fully optimized structure parameters of *a*, *c*, and *u* (*u* = *d*<sub>ap</sub>/*c*; *d*<sub>ap</sub> is the apical Ti–O bond length) for the unit cell of pristine anatase TiO<sub>2</sub> are 3.823 Å, 9.627 Å, and 0.208 respectively, which are in good agreement with experimental results (3.782 Å, 9.502 Å, and 0.208)<sup>33</sup> and other theoretical calculations (3.885, 9.690, 0.208),<sup>24</sup> (3.793, 9.829),<sup>25</sup> and (3.825, 9.678, 0.207).<sup>34</sup> The calculated band gap is 1.98 eV, which is about 1.22 eV smaller than the true value due to the well-known DFT error. GW and TDDFT calculations are able to compute accurate band gaps, but they are very calculation intensive. As we focus only on trends in data obtained for a given dopant in different positions or between chalcogen elements, we expect the GGA band-gap error is largely cancelled.<sup>35</sup>

We used a 2 × 2 × 2 anatase TiO<sub>2</sub> supercell (*a* = *b* = 7.64 Å, *c* = 19.33 Å) containing 96 atoms to simulate the various cases of chalcogen element doping. We substituted either an O atom (substitutional anion doping) or a Ti atom (substitutional cation doping) with a chalcogen element atom or placed a chalcogen element atom at an octahedral interstitial site (interstitial doping). As the ionic radius increases in the order of O<sup>2-</sup> (1.40 Å) << S<sup>2-</sup> (1.84 Å) < Se<sup>2-</sup> (1.98 Å) < Te<sup>2-</sup> (2.24 Å), both cell volume and atomic positions were fully relaxed for substitutional and interstitial anion doping. Hence, the corresponding volume increase is about 1.2, 1.6, 2.2, 2.7, 2.7, and 3.6% for single substitutional and interstitial anionic S, Se, and Te doping, respectively. As the ionic radii of the cationic chalcogen elements straddle the value for Ti<sup>4+</sup> [(0.37 Å (S<sup>4+</sup>), 0.50 Å (Se<sup>4+</sup>), 0.97 Å (Te<sup>4+</sup>), and 0.61 Å for Ti<sup>4+</sup>), we fixed the cell volume and fully relaxed the atomic positions for cationic chalcogen element doping except for Te, where the corresponding volume increase is about 1.5% per Te ion.

For a supercell, the defect formation energy is defined as<sup>36–38</sup>

$$E_f = E_{\text{doped}} - E_{\text{perf}} - n\mu_{\text{dopant}} + m\mu' + qE_F \quad (1)$$

where  $E_{\text{doped}}$  is the total energy of the supercell with the chalcogen element dopant,  $E_{\text{perf}}$  is the total energy of the supercell without the dopant,  $n$  is the number of dopant atoms,  $m$  is the number of O or Ti atoms being removed from the

supercell, ( $n = m$  for substitutional doping, whereas  $m = 0$  for interstitial doping),  $\mu_{\text{dopant}}$  is the chemical potential of the chalcogen element,  $\mu'$  is the chemical potential of O or Ti ( $\mu_{\text{O}}$  or  $\mu_{\text{Ti}}$ ),  $q$  is the charge state of the defect, and  $E_F$  is the Fermi energy of the system. The chemical potential reflects the availability of each element. During simulated growth, if any chemical potential rises above its natural phase value (i.e., that of hcp Ti; O<sub>2</sub> molecule; bulk S, Se, and Te), then the natural phase will form.

In principle, the free energy should be taken as given in eq 1. Use of the (zero-temperature) formation energy implies that contributions from vibrational entropy are neglected. However, estimating vibrational entropy by phonon calculation is too highly demanding on computational resources and time and, so currently, not feasible for the large number of defects to be addressed. Besides, these entropy contributions are small enough not to affect the qualitative results determined by eq 1.<sup>36</sup>

For anatase TiO<sub>2</sub>,  $\mu_{\text{O}}$  and  $\mu_{\text{Ti}}$  must satisfy the following growth condition

$$\mu_{\text{TiO}_2} = \mu_{\text{Ti}} + 2\mu_{\text{O}} \quad (2)$$

where  $\mu_{\text{TiO}_2}$  is the chemical potential of anatase TiO<sub>2</sub>. If the sum on the right-hand side is larger than the left-hand side ( $\mu_{\text{TiO}_2}$ ), the anatase TiO<sub>2</sub> crystal will grow rapidly, whereas if it is lower, the crystal will decompose.

We consider two extreme growth conditions: O-rich and Ti-rich. At O-rich conditions, the chemical potential of O ( $\mu_{\text{O}}$ ) is calculated from the ground-state energy of the O<sub>2</sub> molecule ( $\mu_{\text{O}} = 1/2E_{\text{O}_2}$ ). The chemical potential of Ti ( $\mu_{\text{Ti}}$ ) is then obtained according to eq 2. Conversely, at Ti-rich conditions,  $\mu_{\text{Ti}}$  is calculated from the energy for bulk hcp Ti, and  $\mu_{\text{O}}$  is then obtained.

The chemical potentials of chalcogen elements are calculated according to

$$\mu_X = \mu_{\text{XO}_2} - 2\mu_{\text{O}} \quad (3)$$

where X represents S, Se, and Te. Thus, eqs 2 and 3 are linked through  $\mu_{\text{O}}$ . At O-rich conditions,  $\mu_{\text{S}}$  and  $\mu_{\text{Se}}$  calculated by eq 3 are lower than those of their respective bulk phases. However, the value obtained for  $\mu_{\text{Te}}$  is positive and larger than that of bulk Te; that is, bulk Te is more stable. Thus, the bulk value was used to obtain  $\mu_{\text{Te}}$ . At Ti-rich conditions, the calculated chemical potentials by eq 3 for all three chalcogen elements are positive and larger than those of their bulk phases, indicating that their corresponding bulk S, Se, and Te phases are more stable. Thus, the latter were taken as input to the respective calculation of chemical potentials.

### Results and Discussion

**Interstitial versus Substitutional Doping.** The formation energies for substitutional and interstitial chalcogen element doping in a 96-atom supercell are tabulated in Table 1, as well as plotted as a function of the electronic Fermi energy in Figure 1.

Both neutral and various charged states (2<sup>-</sup>, 1<sup>-</sup>, 0, 1<sup>+</sup>, 2<sup>+</sup>, 3<sup>+</sup>, 4<sup>+</sup>, 5<sup>+</sup>, and 6<sup>+</sup>) of interstitial doping were simulated in this study. The Fermi level ( $E_F$ ) at the valence band maximum (VBM) and at the conduction band minimum (CBM) is set to 0.00 and 3.20 eV, respectively. Moving the Fermi level across the band gap changes the charge state of the interstitial dopant.

**TABLE 1: Formation Energy (eV) of Interstitial and Substitutional Doping in Chalcogen Element-Doped Anatase TiO<sub>2</sub> with the Fermi Level at the VBM**

dopant	O-rich			Ti-rich		
	S	Se	Te	S	Se	Te
X@O (anion)	7.88	7.43	8.07	0.88	1.56	3.49
X@Ti (cation)	2.61	-0.11	-2.76	9.62	8.03	6.67
1 <sup>-</sup>	9.53	8.80	9.61	7.11	7.51	9.61
2 <sup>-</sup>	12.13	11.40	12.70	9.71	10.11	12.70
neutral	7.15	6.42	6.63	4.73	5.13	6.63
1 <sup>+</sup>	6.00	5.24	3.78	3.58	3.94	3.78
2 <sup>+</sup>	3.12	1.95	1.07	0.71	0.66	1.07
3 <sup>+</sup>	1.56	0.22	-1.52	-0.86	-1.08	-1.52
4 <sup>+</sup>	-0.44	-1.17	-3.90	-2.86	-2.46	-3.90
5 <sup>+</sup>	-1.37	-2.17	-5.06	-3.79	-3.46	-5.06
6 <sup>+</sup>	-1.35	-3.56	-7.21	-3.76	-4.85	-7.21

The charge state changes from 6<sup>+</sup> → 5<sup>+</sup> → 4<sup>+</sup> → 0 → 1<sup>-</sup> → 2<sup>-</sup> for S, 6<sup>+</sup> → 4<sup>+</sup> → 2<sup>+</sup> → 0 → 1<sup>-</sup> → 2<sup>-</sup> for Se, and 6<sup>+</sup> → 4<sup>+</sup> →

3<sup>+</sup> → 2<sup>+</sup> → 1<sup>+</sup> → 0 for Te dopants. The thermodynamic transition level (TRL) between two different charged states ( $q_1/q_2$ ) is defined as the Fermi level position where both charged states of  $q_1$  and  $q_2$  have the same formation energy. The TRLs for various interstitial chalcogen element dopants are shown in Figure 2. The TRL from the neutral to the nearest positively charged state for interstitial S, Se, and Te dopants is 2.35, 2.62, and 3.18 eV, respectively, that is, 0.85, 0.58, and 0.02 eV below the CBM, respectively, indicating that S and Se are deep donors, whereas Te is a shallow donor. The TRL from the neutral to the nearest negatively charged state for interstitial S, Se, and Te dopants is 2.71, 2.71, and 3.32 eV above the VBM, respectively, showing that these dopants are deep acceptors.

To answer whether interstitial doping of TiO<sub>2</sub> by chalcogen elements is possible, we analyzed the relationship between formation energy of various species and the Fermi level under two growth conditions, as depicted in Figure 1. TiO<sub>2</sub> is a native

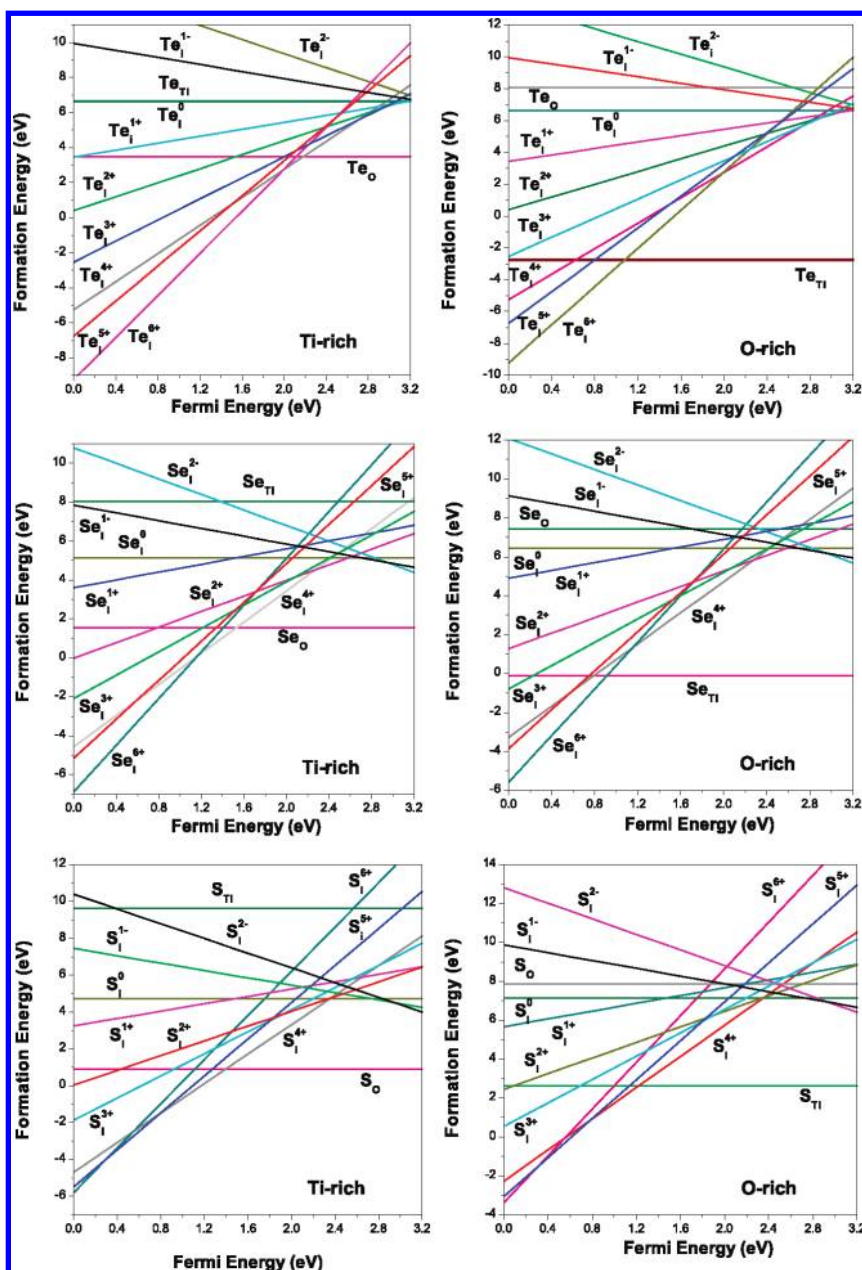


**Figure 1.** Formation energies of interstitial and substitutional doping as a function of the Fermi level, under the Ti-rich (left panel) and O-rich (right panel) growth conditions, respectively. The slope of the line is an indication of the charge state of the dopant. The Fermi energy, reference to the top of the valence band, is all the way to the experimental band gap.

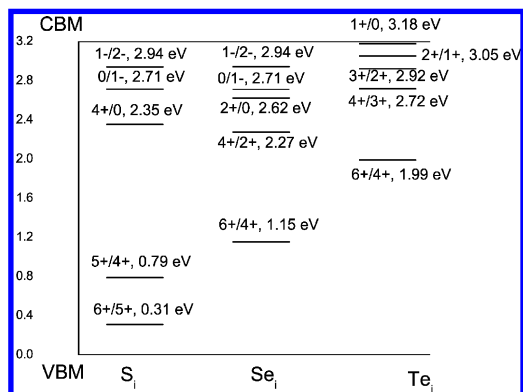


**Figure 2.** Thermodynamic transition levels (TRLs) for various dopant types in chalcogen element-doped  $\text{TiO}_2$ , determined from formation energies; see main text for details.

n-type semiconductor. At n-type conditions (i.e.,  $E_F$  is closer to the CBM), as shown in Figure 1, substitutional doping is the most stable dopant type. Under p-type conditions (i.e.,  $E_F = 0$ , at the top of the VBM), the formation energies of interstitial chalcogen elements ( $\text{S}_i$ ,  $\text{Se}_i$ , and  $\text{Te}_i$ ) are negative under both Ti- and O-rich conditions. These formation energies remain negative as long as  $E_F$  is lower than 0.83, 0.81, and 1.20 eV under Ti-rich conditions or 0.27, 0.59, and 1.20 eV under O-rich condition, respectively. A negative energy means that the formation of the defect is spontaneous; that is, under p-type conditions, these chalcogen elements will occupy interstitial positions and immediately donate electrons to the surrounding atoms, making  $E_F$  move away from the VBM and toward the

CBM. The rapid formation of these charged donors thus quickly converts the chalcogen element-doped  $\text{TiO}_2$  to n-type. Under n-type conditions, the most stable dopant is substitutional. Therefore, it is impossible to produce interstitial chalcogen element-doped anatase  $\text{TiO}_2$  under any equilibrium growth condition. Thus, we will restrict our remaining discussion to substitutional doping.

To verify that the 94-atom  $2 \times 2 \times 2$  supercell was an adequate model, simulations of various types of chalcogen element doping into a  $3 \times 3 \times 1$  anatase  $\text{TiO}_2$  supercell were also made and compared. This larger supercell contains 108 atoms and is more nearly equiaxial ( $a = b = 11.46 \text{ \AA}$  and  $c = 9.67 \text{ \AA}$ ). Formation energies were very similar in both models except for the one case of anionic substitutional doping, where the energies were roughly 0.5 eV lower in the  $3 \times 3 \times 1$  supercell, viz., 0.43, 1.07, and 2.94 eV for S, Se, and Te, respectively. Nevertheless, the systematic trend across the chalcogen element series was clearly consistent in both, demonstrating that the  $2 \times 2 \times 2$  supercell is adequate.

**Substitutional Doping.** At O-rich conditions, the formation energies of cationic (substitutional) doping are much lower than those for anionic (substitutional) doping, indicating that the chalcogen element prefers to substitute for Ti. The formation energy decreases with increasing atomic number of the chalcogen element, indicating that it is easier to dope cationic Se and Te than cationic S. The formation energy for cationic S doping is 2.61 eV, which is slightly lower than the value Dai et al reported (3.20 eV).<sup>26</sup> The formation energies for cationic Se and Te doping are negative, suggesting that it should be easy to prepare substitutional cationic Se- or Te-doped anatase  $\text{TiO}_2$

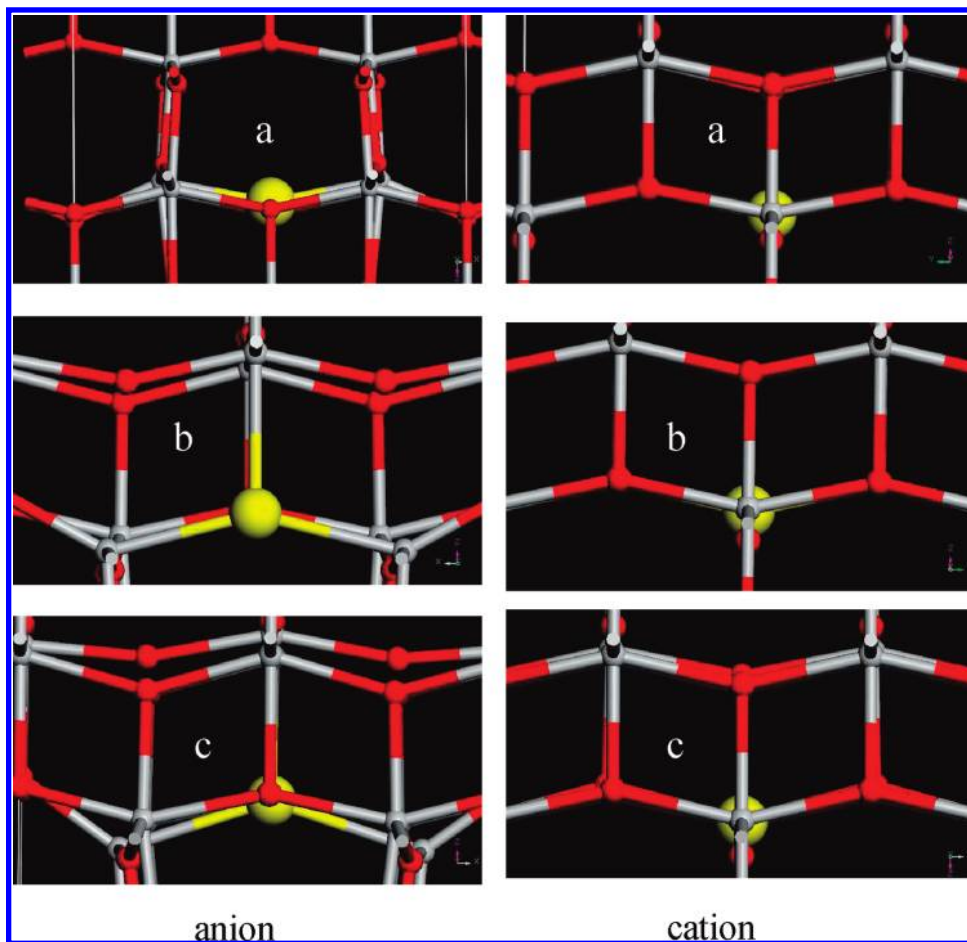


**Figure 3.** Partial geometry for anion (left panel) and cation (right panel) doped  $\text{TiO}_2$ : (a) S doping, (b) Se doping, and (c) Te doping.

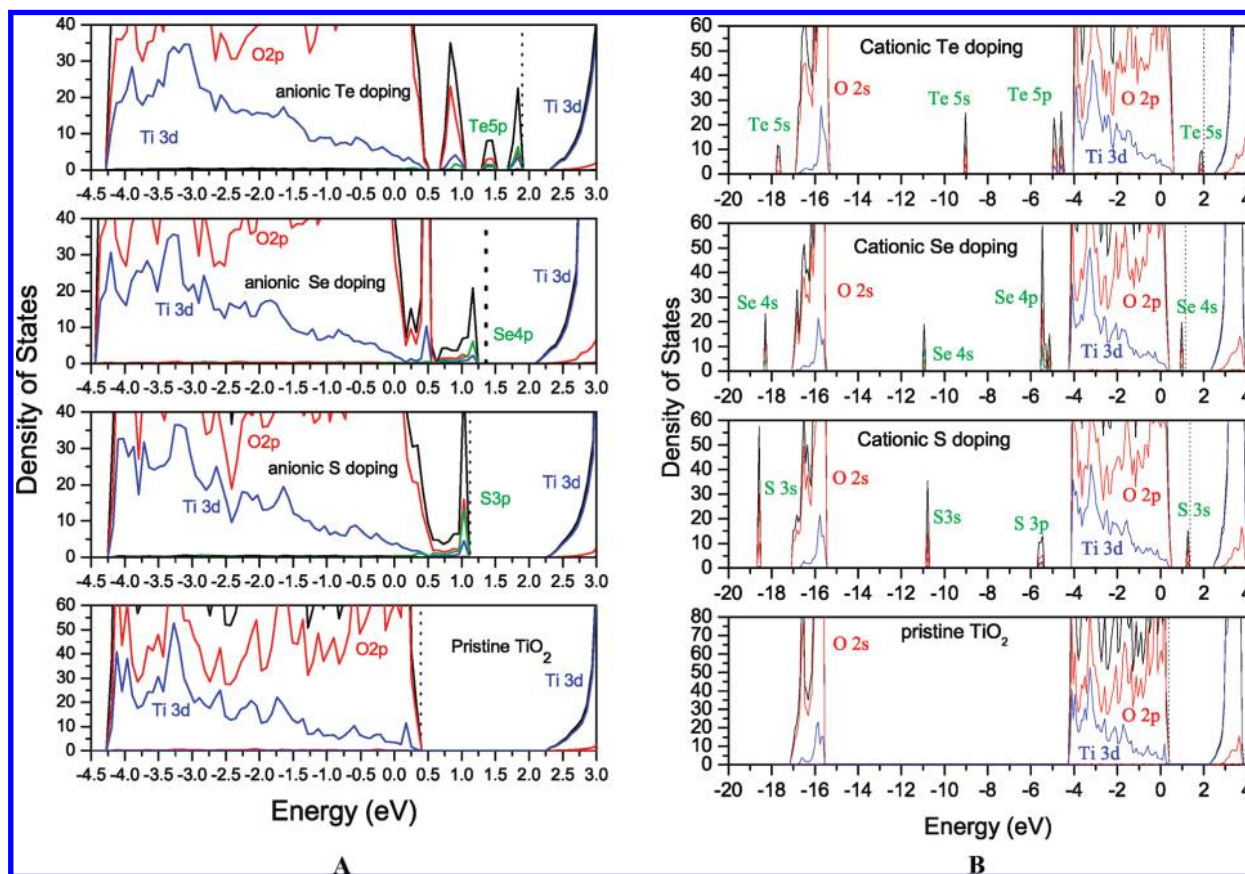


**Figure 4.** Partial density of states for various substitutional chalcogen element-doped TiO<sub>2</sub>: (A) anion doping and (B) cation doping. The dashed line indicates the position of the Fermi level.

at O-rich conditions. Conversely, under Ti-rich conditions, the formation energies of anionic doping are much lower than those of cationic doping, indicating that chalcogen elements now prefer to substitute for O. The formation energy increases in the order of S < Se < Te, showing that it is progressively harder to prepare anionic Se- and Te-doped anatase TiO<sub>2</sub>. The formation energy for anionic S doping is 0.88 eV, which is much lower than the value reported by Dai et al (3.80 eV)<sup>26</sup> because we used the more reasonable chemical potential ( $\mu_s$ ) calculated from bulk sulfur and as compared to sulfur dioxide.

The trend in the formation energies of chalcogen element(s)-doped TiO<sub>2</sub> seen in this work is in line with the trend in their ionic radii and electronegativity. With increasing atomic number, the ionic radius increases, whereas the electronegativity decreases; that is, cationic forms will become more stable relative to anionic forms. The higher stability of Te<sup>4+</sup> as compared with Te<sup>2+</sup> is well-known.

The partial geometries taken from the optimized structures are shown in Figure 3. Because of the larger ionic radii of the chalcogen elements in the anionic form as compared with O<sup>2-</sup> (1.84, 1.98, 2.21, and 1.40 Å for S<sup>2-</sup>, Se<sup>2-</sup>, Te<sup>2-</sup>, and O<sup>2-</sup>, respectively), the chalcogen tends to push the three bonding Ti atoms outward. The optimized X–Ti bond lengths are 2.197 and 2.327, 2.293 and 2.409, and 2.455 and 2.555 Å for X = S, Se, and Te, respectively, which are longer than the O–Ti bond lengths in pristine TiO<sub>2</sub> (1.955 and 2.003 Å). In contrast, the influence on the structure of cationic doping is not as obvious as anionic doping, due to the much smaller ionic radii of the cations as compared with the anions. The optimized X–O bond lengths are 1.926 and 1.915, 1.987 and 2.030, and 2.057 and 2.151 Å for X = S, Se, and Te, respectively.

The partial density of states for substitutional anionic doping with chalcogen elements is shown in Figure 4A. S 3p and Se 4p orbitals both appear at the top of the VBM and mix with O 2p orbitals. Se doping induces an obvious O 2p/Ti 3d shoulder peak, which is absent in S doping, and the Se states extend more into the band gap than S states. However, Te 5p orbitals split into three localized gap states that are almost evenly distributed across the gap. The Fermi level is pinned above these localized states, indicating that they are occupied. Hence, optical excitation from these occupied states to the CBM should occur from well into the visible region. The theoretical gap from those occupied states to the CBM is 1.21, 0.80, and 0.48 eV for anionic S, Se, and Te doping, respectively, which are much smaller than that of pristine TiO<sub>2</sub> (1.98 eV). Thus, anionic doping with heavier chalcogen elements is more effective to shifting the absorption edge into the visible region. Our calculation result for anionic S doping is consistent with the experimental work of Ho et al.<sup>35</sup> They observed the obvious enhancement of the absorption from about 400 to 560 nm, which corresponds to band-gap narrowing of the order of 0.89 eV. Our calculated value is 0.77 eV.

In contrast, cationic chalcogen element doping induces sharp and localized gap states (see Figure 4B). These originate from s states of the chalcogen element dopant and 2p states of the adjacent O atoms bonding to the dopant. It is 0.83, 0.65, and 1.37 eV above the VBM for S, Se, and Te, respectively. The p states of the chalcogen element dopants do not appear in the band gap and are localized at a lower energy range (<−4.5 eV). The VBM and CBM edges of anatase TiO<sub>2</sub> are almost unchanged upon doping with cationic Se, whereas cationic S and Te doping raises the VBM edge by 0.1 and 0.21 eV and

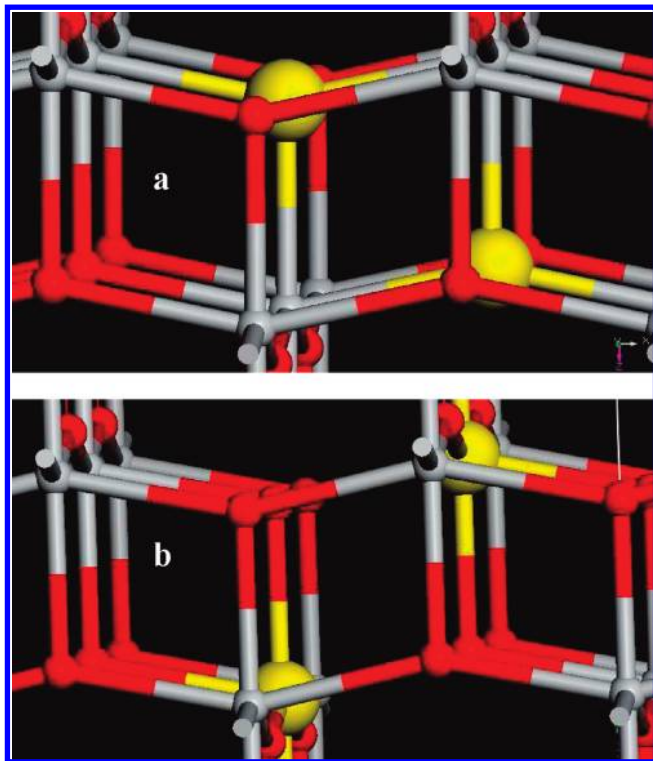


**Figure 5.** Dopant pairing in substitutional chalcogen element-doped  $\text{TiO}_2$ : (a) anion–anion and (b) cation–cation.

the CBM edge by 0.18 and 0.23 eV, respectively. The Fermi level is pinned above these sharp localized gap states, indicating that they are occupied. The theoretical gap from these occupied gap states to the CBM is 1.25, 1.39, and 0.64 eV for cationic S, Se, and Te doping, respectively. Therefore, the excitation of electrons from these occupied gap states should also induce visible light absorption. Our results agree very well with Ohno's work<sup>23</sup> reporting new absorption from 410 to 550 nm. This corresponds to a band-gap narrowing of  $\sim 0.77$  eV, as compared to our calculated red shift of 0.73 eV.

**Dopant Pairing.** It is well-known that sulfur atoms tend to self-associate (catenation). Hence, it was considered of interest to include this aspect in the current study, that is, to evaluate any tendency of the chalcogen elements in general to pair up or form localized clusters in  $\text{TiO}_2$ . The foregoing calculations have already determined a very low probability of finding dopants in interstitial sites and indicated that anionic and cationic chalcogen element dopants are not able to coexist under any equilibrium growth conditions. Thus, we considered the following two pairing patterns. The first is anion–anion pairing, in which the two dopant atoms substitute for a pair of nearest-neighbor O atoms, as shown in Figure 5a. The optimized distance between the two dopant anions in the case of S, Se, and Te is 3.033, 3.091, and 2.732 Å, respectively. The second pattern is the corresponding case of adjacent cation–cation pairing (see Figure 5b). The optimized distance between the two dopant cations for S, Se, and Te is 3.231, 3.246, and 3.334 Å, respectively.

Pairing energy is defined as follows

$$E_{\text{pair}} = (E_{2\text{D}} - E_{\text{perf}}) - 2^*(E_{1\text{D}} - E_{\text{perf}})$$

where  $E_{1\text{D}}$  and  $E_{2\text{D}}$  are the total energy of the supercell having one and two dopants, respectively.  $E_{\text{perf}}$  is the total energy of

**TABLE 2: Pairing Energy (eV) for Various Chalcogen Element Dopants in Chalcogen Element-Doped Anatase  $\text{TiO}_2$**

	anion–anion		cation–cation	
	nearest	separated	nearest	separated
S–S	–1.28 (3.0 Å) <sup>a</sup>	–1.23 (5.6 Å)	–3.10 (3.2 Å)	–2.69 (7.4 Å)
Se–Se	–2.04 (3.1 Å)	–1.42 (5.6 Å)	0.18 (3.2 Å)	
Te–Te	–4.45 (2.7 Å)	–1.80 (5.3 Å)	0.53 (3.3 Å)	

<sup>a</sup> The number in the bracket is the distance between the two dopant atoms.

the supercell without any dopant. By definition, negative pairing energy means that the dopants have a finite probability (tendency) to associate. The calculated pairing energies are listed in Table 2. It is interesting to note that the pairing energies for S in both anionic and cationic forms is always negative (even when the two dopants are separated about 7.4 Å), indicating that S tends to pair up in either case. The corresponding pairing energies for cationic Se and Te dopants is 0.18 and 0.53 eV, respectively, when they are at the nearest positions, indicating that cationic Se and Te dopants do not tend to pair. In contrast, the pairing energies for anionic Se and Te dopants is –2.04 and –4.45 eV, respectively, showing that anionic Se and Te dopants like to pair up even more than anionic S. The larger pairing energy for the Te dopant is driven by the formation of a chemical bond between the two Te dopant atoms (the optimized distance between the two Te atoms is 2.732 Å). When the two dopant atoms are separated at about 5.3 Å, the pairing energy for anionic Se and Te dopants is still negative, (–1.42 and –1.80 eV, respectively), indicating that all anionic chalcogen element dopants tend to pair up.

Dopant pairing also affects the electronic structure of  $\text{TiO}_2$ . The partial density of states for various nearest-neighbor dopant pairings is shown in Figure 6. The DOS in Figure 6 is quite different from the corresponding DOS for single substitutional dopants (see Figure 4). Anionic dopant pairing causes the dopant gap states to split into four gap states that are all occupied. The theoretical gap between these occupied gap states and the CBM for anionic S and Se dopant pairing is significantly reduced, whereas for anionic Te pairing, it is increased slightly, possibly due to the formation of the Te–Te bond. Thus, anionic dopant pairing may also confer visible light absorption properties into the chalcogen element-doped  $\text{TiO}_2$ .

The influence of cationic S dopant pairing is very interesting. Single cationic S doping generates a sharp 3s gap state lying toward the center of the band gap (please refer to Figure 4). However, the cationic S dopant pair generates occupied gap states just above the VBM, which is similar to what is observed in the single anionic S doping. As a result, the theoretical gap is 0.28 eV larger than that of single cationic S doping, which corresponds to a blue shift in the absorption edge of the order of 50 nm. Therefore, cationic S dopant pairing is a process that should be avoided. This is confirmed by recent independent experimental observations.<sup>39,40</sup> The UV–vis absorption of cationic S-doped  $\text{TiO}_2$  was blue shifted when the S content exceeded 4% (Figure 8 in ref 39) or when the initial mass ratio of thiourea/ $\text{TiO}_2$  exceeded 5/1 (Figure 10 in ref 40).

## Conclusion

In summary, the prospects of sensitizing  $\text{TiO}_2$  to visible light by the doping of chalcogen elements has been evaluated by first-principles DFT calculations. Various substitutional doping configurations look favorable, introducing filled gap states that should result in band-gap narrowing. Interstitial doping is not

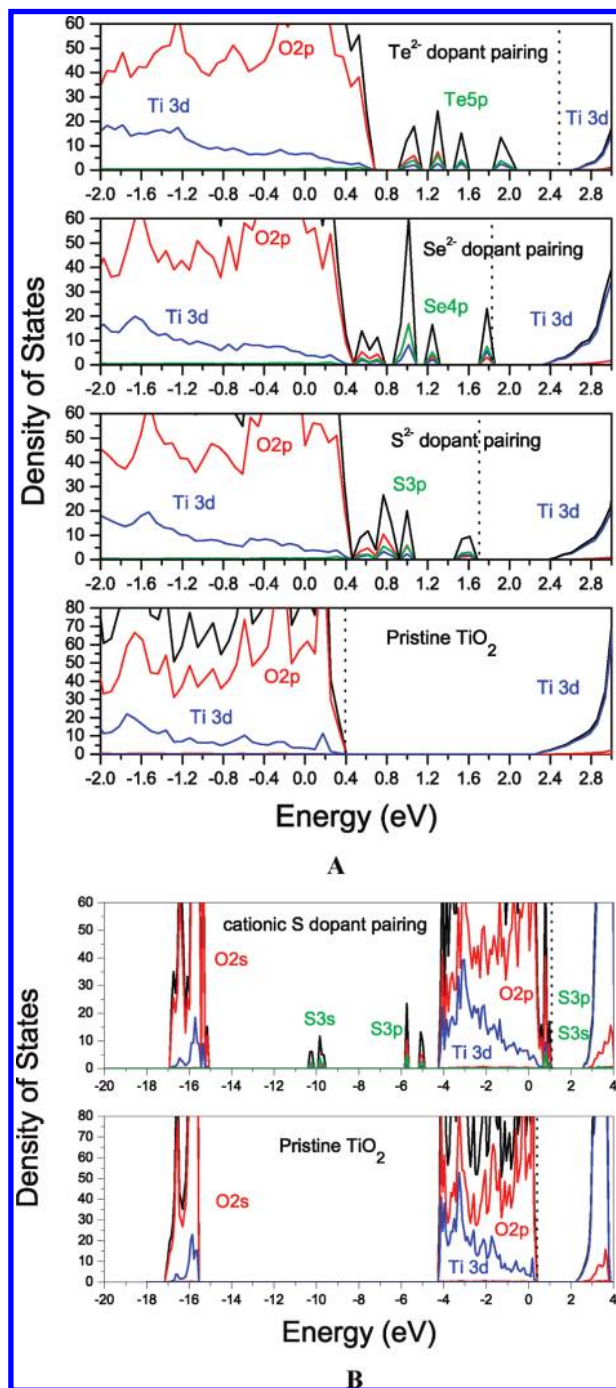


**Figure 6.** Partial density of states for various dopant pairings in substitutional chalcogen element-doped TiO<sub>2</sub>: (A) anion–anion and (B) cation–cation. The dashed line indicates the position of the Fermi level.

possible under any equilibrium growth condition. Anion substitutional doping by S, Se, and Te is more effective than cation doping, while the red shift increases progressively with increasing atomic number of the chalcogen element. Both anionic and cationic S dopants tend to pair up, but only anionic dopant pairs are favorable for sensitization purposes. For Se and Te, only anionic Se and Te dopants pair up, and these also favor sensitization to visible light.

**Acknowledgment.** The authors gratefully acknowledge research funding support from the Agency for Science, Technology and Research (A\*STAR), Singapore (PSF0521010016), support received from the Institute of High Performance Computing (A\*STAR), and fruitful discussions with Dr. Yu Zhigen.

## References and Notes

- (1) Fujishima, A.; Honda, K. *Nature* **1972**, *238*, 37.
- (2) Ashokkumar, M. *Int. J. Hydrogen Energy* **1998**, *23*, 427.
- (3) Ni, M.; Leung, M. K. H.; Leung, D. Y. C.; Sumathy, K. *Renewable Sustainable Energy Rev.* **2007**, *11*, 401.
- (4) Osterloh, F. E. *Chem. Mater.* **2008**, *20*, 35.
- (5) Han, F.; Kambala, V. S. R.; Srinivasan, M.; Rajarathnam, D.; Naidu, R. *Appl. Catal., A* **2009**, *359*, 25.
- (6) Singh, A. P.; Kumari, S.; Shrivastav, R.; Dass, S.; Satsangi, V. R. *Int. J. Hydrogen Energy* **2008**, *33*, 5363.
- (7) Shao, G. *J. Phys. Chem C* **2008**, *112*, 18677.
- (8) Sasikala, R.; Sudarsan, V.; Sudakar, C.; Naik, R.; Sakuntala, T.; Bharadwaj, S. R. *Int. J. Hydrogen Energy* **2008**, *33*, 4966.
- (9) Seery, M. K.; George, R.; Floris, P.; Phillai, S. C. *J. Photochem. Photobiol., A* **2007**, *189*, 258.
- (10) Kim, S.; Hwang, S.-J.; Choi, W. *J. Phys. Chem. B* **2005**, *109*, 24260.
- (11) Emeline, A. V.; Kuzmin, G. N.; Serpone, N. *Chem. Phys. Lett.* **2008**, *454*, 279.
- (12) Asahi, R.; Morikawa, T.; Ohwaki, T.; Aoki, K.; Taga, Y. *Science* **2001**, *293*, 269.
- (13) Asahi, R.; Morikawa, T. *Chem. Phys.* **2007**, *339*, 57.
- (14) Long, M. C.; Cai, W. M.; Wang, Z. P.; Liu, G. Z. *Chem. Phys. Lett.* **2006**, *420*, 71.
- (15) Lin, Z. S.; Orlov, A.; Lambert, R. M.; Payne, M. C. *J. Phys. Chem. B* **2005**, *109*, 20948.
- (16) Yang, K. S.; Dai, Y.; Huang, B. B. *J. Phys. Chem. C* **2007**, *111*, 12086.
- (17) Sathish, M.; Viswanathan, B.; Viswanath, R. P.; Gopinath, C. S. *Chem. Mater.* **2005**, *17*, 6349.
- (18) Di Valentin, C.; Pacchioni, G.; Selloni, A. *Chem. Mater.* **2005**, *17*, 6656.
- (19) Zaleska, A.; Sobczak, J. W.; Grabowska, E.; Hupka, J. *Appl. Catal., B* **2008**, *78*, 92.
- (20) Yang, K. S.; Dai, Y.; Huang, B. B.; Whangbo, M. H. *Chem. Mater.* **2008**, *20*, 6528.
- (21) Liu, G.; Chen, Z. G.; Dong, C. L.; Zhao, Y. N.; Li, F.; Lu, G. Q.; Cheng, H. M. *J. Phys. Chem. B* **2006**, *110*, 20823.
- (22) Umebayashi, T.; Yamaki, T.; Itoh, H.; Asai, K. *Appl. Phys. Lett.* **2002**, *81*, 454.
- (23) Ohno, T.; Akiyoshi, M.; Umebayashi, T.; Asai, K.; Mitsui, T.; Matsumura, M. *Appl. Catal., A* **2004**, *265*, 115.
- (24) Tian, F. H.; Liu, C. B. *J. Phys. Chem. B* **2006**, *110*, 17866.
- (25) Matsushima, S.; Takehara, K.; Yamane, H.; Yamada, K.; Nakamura, H.; Arai, M.; Kobayashi, K. *J. Phys. Chem. Solids* **2007**, *68*, 206.
- (26) Yang, K. S.; Dai, Y.; Huang, B. B. *J. Phys. Chem. C* **2007**, *111*, 18985.
- (27) Nishijima, K.; Fujisawa, Y.; Murakami, N.; Tsubota, T.; Ohno, T. *Appl. Catal., B* **2008**, *84*, 584.
- (28) Kresse, G.; Hafner, J. *Phys. Rev. B* **1993**, *48*, 13115.
- (29) Kresse, G.; Hafner, J. *Phys. Rev. B* **1994**, *49*, 14251.
- (30) Blochl, P. E. *Phys. Rev. B* **1994**, *50*, 17953.
- (31) Kresse, G.; Joubert, D. *Phys. Rev. B* **1999**, *59*, 1758.
- (32) Perdew, J. P.; Wang, Y. *Phys. Rev. B* **1992**, *45*, 13244.
- (33) Burdett, J. K.; Hughbank, T.; Miller, G. J.; Ricardson, J. W.; Smith, J. V. *J. Am. Chem. Soc.* **1987**, *109*, 3639.
- (34) Geng, W. T.; Kima, K. S. *Solid State Commun.* **2004**, *129*, 741.
- (35) Ho, W. K.; Yu, J. C.; Lee, S. C. *J. Solid State Chem.* **2006**, *179*, 1171.
- (36) Van de Walle, C. G.; Neugebauer, J. *J. Appl. Phys.* **2004**, *95*, 3851.
- (37) Laks, D. B.; Van de Walle, C. G.; Neumark, G. F.; Pantelides, S. T. *Phys. Rev. Lett.* **1991**, *66*, 648.
- (38) Zhang, S. B.; Northrup, J. E. *Phys. Rev. Lett.* **1991**, *67*, 2339.
- (39) Hamadani, M.; Reisi-Vanani, A.; Majedi, A. *Mater. Chem. Phys.* **2009**, *116*, 376.
- (40) Znad, H.; Kawase, Y. *J. Mol. Catal. A: Chem.* **2009**, *314*, 55.